Physics of Fluids

RESEARCH ARTICLE | MAY 24 2024

Optimal strategy of the asymmetric wave energy converter survival in extreme waves

Binzhen Zhou (周斌珍) ; Yi Xiao (肖义) ; Kanglixi Ding (丁康礼玺) ; Lei Wang (王磊) ; Yifeng Yang (杨毅锋) ; Peng Jin (金鹏)

Physics of Fluids 36, 057146 (2024)
https://doi.org/10.1063/5.0208825

Physics of Fluids ARTICLE pubs.aip.org/aip/pof

Optimal strategy of the asymmetric wave energy converter survival in extreme waves

Cite as: Phys. Fluids **36**, 057146 (2024); doi: 10.1063/5.0208825
Submitted: 17 March 2024 · Accepted: 9 May 2024 ·
Published Online: 24 May 2024

Binzhen Zhou (周斌珍),[1,2] Yi Xiao (肖义),[2] Kanglixi Ding (丁康礼玺),[2] Lei Wang (王磊),[2,3,4,a)] Yifeng Yang (杨毅锋),[5] and Peng Jin (金鹏)[2]

AFFILIATIONS

[1]State Key Laboratory of Subtropical Building and Urban Science, South China University of Technology, Guangzhou 510641, China
[2]School of Civil Engineering and Transportation, South China University of Technology, Guangzhou 510641, China
[3]Guangdong Provincial Key Laboratory of Marine Disaster Prediction and Prevention, Shantou University, Shantou 515063, China
[4]Department of Civil and Environment Engineering, The Hong Kong Polytechnic University, Hong Kong 999077, China
[5]Department of Mechanical Engineering, University College London, Torrington Place, London WC1E 7JL, United Kingdom

[a)]**Author to whom correspondence should be addressed:** wangleimme@scut.edu.cn

ABSTRACT

Enhancing the survival performance of wave energy converters (WECs) in extreme wave conditions is crucial, and reducing wave loads is a key aspect of this. Placing the device underwater has been recognized as a beneficial strategy, yet the determination of the optimal submerged depth and the effects of varying wave conditions remain ambiguous. To address this, the study numerically analyzes the total forces in both horizontal and vertical directions, along with their harmonic components, across different wave configurations. A computational fluid dynamics method is employed to investigate a triangular-baffle bottom-shaped oscillating floater, which is known for its high energy conversion efficiency. The findings indicate that submerging the device to a depth equivalent to half the actual focused amplitude ($1/2A_b$) is the most effective strategy in the given sea state, offering superior wave force reduction vertically and robust performance horizontally. The analysis of harmonics reveals the significant contribution of high-order components to the total wave forces. Additionally, the study examines the impact of focused wave amplitudes and peak frequencies, showing that although force reductions are lessened in more extreme conditions, the optimal submerged depth of $1/2A_b$ still yields near 30% reduction in total vertical force and 22% in total horizontal force. This research provides theoretical insight that can guide the enhancement of WECs' survival capabilities in practical engineering applications.

I. INTRODUCTION

Wave energy holds significant potential as a renewable energy due to its widespread availability, substantial reservation, and predictability.[1,2] In recent decades, over a thousand wave energy converters (WECs) have been proposed, including types such as oscillating buoy type,[3,4] oscillating water column type,[5,6] and overtopping type.[7,8] Beyond their ability to generate power under normal operating conditions, their survival capacity in extreme sea conditions is a critical factor in assessing their overall. Extreme waves,[9,10] which are characterized by their strong nonlinearity and concentrated energy, present a formidable challenge, with the potential to damage or even destroy these devices. Consequently, enhancing the ability of WECs to withstand extreme wave conditions is of paramount importance.

In working mode, the WECs generate electricity by the relative heave motion forced by power takeoff (PTO). Extensive research has focused on optimizing wave energy converters renowned for their superior energy conversion efficiency. Findings have demonstrated a strong correlation between this efficiency and the design of the floater's bottom shape.[11,12] The oscillating-buoy WEC, known for its flexible configuration and ease of construction,[13,14] is a popular choice in wave energy conversion. Research by Zhou *et al.*[15] using the semi-analytical solution revealed that floaters with symmetrical bottom shapes[16,17] outperform those with symmetrical designs in terms of energy conversion efficiency, and the greater the asymmetry, the higher the efficiency. Madhi *et al.*[18] introduced an asymmetrical design named "Berkeley Wedge," which achieved an impressive energy conversion efficiency of up to 96.34% under ideal conditions. Building on this, Zhang *et al.*[19] developed a "triangular-baffle" bottom shape, which demonstrated a comparably high efficiency of 93%. This finding has been corroborated by the studies of Wei *et al.*[20] and Cheng *et al.*[21]

Given these advancements, it is essential to investigate the survivability of floater with a triangular-baffle shaped bottom to ensure their practical application in wave energy projects.

However, in extreme sea conditions, the WECs should stop working and even be placed underwater to avoid the impact of the large wave loads, which is known as the survival mode. The resilience of WECs under such conditions has increasingly become a focus of academic research. Weller *et al.*[22] performed laboratory experiments to analyze the motion response of a WEC and observed that the horizontal displacement (i.e., in the direction of wave propagation) could exceed the vertical displacement by more than six times immediately after passing the focus point of the waves. Sirigu *et al.*[23] experimented with a 1:20 scale model of the Inertial Sea Wave Energy Converter (ISWEC) and discovered that adding a clump weight to the mooring line significantly reduced mooring loads and lowered peak values. Shahroozi *et al.*[24] conducted a 1:30 scale experiment to explore how PTO damping parameters affect the mooring loads of a point absorber during extreme wave events. However, the motion response of WECs can become excessively large under extreme waves. Ropero *et al.*[25] suggested a proactive strategy to mitigate disaster losses by submerging fixed WECs, based on a comparison of horizontal and vertical forces on a heaving point absorber with PTO using the Smoothed Particle Hydrodynamics (SPH) numerical method. This approach was supported by Madhi and Yeung,[26] who studied wave loads on a floater with a Berkeley Wedge-shaped bottom in extreme breaking waves. While submergence is considered an effective survival strategy, the optimal depth of submergence and the influence of wave configurations remain unclear. Additionally, research on wave loads has been limited to the analysis of total force.

Under extreme waves wave conditions characterized by strong nonlinearities, the resultant high-order wave forces inflict significant damage on devices, a factor that cannot be overlooked. Drawing inspiration from the successful application of phase decomposition in focused waves,[27,28] Zang *et al.*[29] employed a two-phase decomposition method to analyze wave loads on a cylinder with a perforated surface, demonstrating the validity of this approach for decomposing hydrodynamic loads. Chen *et al.*[30] isolated the higher-order forces acting on cylinders and discovered that these components accounted for more than 60% of the forces in the specified wave configuration. Subsequently, Fitzgerald *et al.*[31] proposed a four-phase decomposition method, which allows the wave spectrum to be extended wider. Following this advancement, Feng *et al.*[32] explained the higher order forces and moments on the cylinder with the surface perforated dominated by inertia and pointed out that the higher-harmonic moments are relatively larger with more enhanced nonlinearity.

The aforementioned research indicates that placing the floater underwater can effectively reduce the load force, being an accepted positive strategy for enhancing survival in extreme wave conditions. However, the determination of the optimal submergence depth and the effects of wave configuration on this strategy remain unresolved. To address these gaps, this study conducts a numerical investigation of the total forces in the horizontal and vertical directions, as well as their harmonic components, at various submerged depths. The novelties are threefold. First, the variations of the vertical and horizontal forces influenced by the submerged depth are clearly explained. Second, it identifies the predominant components within the total wave force through harmonic analysis. Third, it determines an optimal submerged depth for withstanding extreme wave conditions and examines the influence of wave configurations on this depth.

The rest of the paper is arranged as follows. Section II introduces the methodology of the numerical model. Section III describes the numerical setup and conducts the modal validation. Results and analysis are given in Sec. IV. The conclusions are summarized in Sec. V.

II. METHODOLOGY

A. Flow field model

A computational fluid dynamics (CFD) method is applied hereafter to simulate the marine device in extreme wave conditions. The numerical wave tank is established based on the software STAR-CCM+.[33] The laminar flow model, which has been successfully applied in the study of Zhang *et al.*[19] on the power generation performance of floaters for its higher computational accuracy and efficiency in dealing with such issues, is adopted in this study to simulate the wave loads on a floater with a triangular-baffle-shaped bottom. The fluid is assumed to be Newtonian and incompressible. As sketched in Fig. 2, the origin of a coordinate system is arranged to be located at the still water surface on the left boundary, and the direction of the wave propagation is defined as the positive of the x axis, with vertical upward as the positive of the z axis. The corresponding continuity equation is written as

$$\nabla \cdot \mathbf{u} = 0, \tag{1}$$

where $\nabla = (\partial/\partial x, \partial/\partial z)$, and $\mathbf{u} = (u_x, u_z)$ denotes the velocity vector.

The momentum equation is expressed as

$$\frac{\partial \mathbf{u}}{\partial t} + \mathbf{u} \cdot \nabla \mathbf{u} = \mathbf{g} - \frac{1}{\rho}\nabla p + \frac{\mu}{\rho}\nabla^2 \mathbf{u}, \tag{2}$$

where t is the time, ρ is the fluid density, p is the fluid pressure, μ is the dynamic viscosity, and $\mathbf{g} = (0, -g)$ is a vector of the gravitational acceleration.

The governing equations are discretized and numerically solved through the finite volume method (FVM), and the volume of fluid (VOF) method is applied to capture the free surface interface between air and water. Detailed supplements can be found in Ref. 34.

The inlet boundary on the left and the outlet boundary on the right of the numerical tank are set up as the velocity inlet boundary condition, in which the velocity vector on the boundary surface is the velocity of a specified wave and its composition of fluid components is set to be a two-phase flow of water and air. The top boundary of the numerical tank is set as the pressure outlet boundary, in which the pressure on the pressure outlet boundary surface is the hydrostatic pressure of a specified wave, and the working fluid is air. Both lateral boundaries of the numerical wave tank satisfy the symmetry plane boundary condition. The bottom and the surface of the floater satisfy the wall boundary condition, in which the fluid velocity at the fixed wall is set as zero.

The mesh refinements are performed in the entire fluid domain, and there are two main regions, one is near the free surface (named the liquid level encryption zone) and the other is around the floater (named the floating body encryption zone). The overview of the mesh in the fluid domain is given in Fig. 1.

B. Wave absorption

The wave forcing method is used for wave absorption. A source term q_ϕ is added to the momentum equation to force the solution of

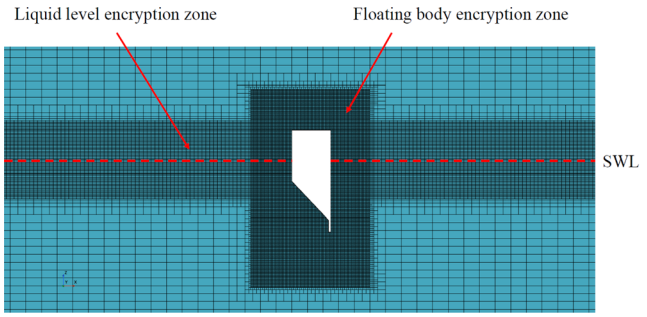

FIG. 1. Mesh refinement of the liquid level encryption and floating body encryption zone.

the Navier–Stokes equations toward the theoretical solution or to a simplified numerical solution within a specified distance:[35]

$$q_\phi = -\gamma\rho(\phi - \phi^*), \tag{3}$$

where ϕ is the current solution to the momentum equation, and ϕ^* is the value toward which the solution is forced. γ is the forcing coefficient, expressed as

$$\gamma = -\gamma_0 \cos^2(\pi x^*/2), \tag{4}$$

in which γ_0 is the maximum value, and x^* is the distance from the inner edge to the outer edge of the forcing zone.

C. Wave generation

Focused waves are generated by the superstition of the VOF module, and the wave forcing method is also applied at the left boundary in front of the wavemaker to ensure the incident waves. The period T_i of the ith wave component can be calculated from

$$T_i = 1/f_i. \tag{5}$$

Supposed that the wave components are focused at the assumed focused position $x = x_{ab}$ and the assumed focused time $t = t_{ab}$, it can be regarded[36]

$$\cos(2\pi f_i t_{ab} - k_i x_{ab} + \phi_i) = 1, \tag{6}$$

TABLE I. The positions of the floater in the survival state.

Case	Distance between the top of the floater and SWL d	The corresponding state
LC1	$-A_b$	Emerged
LC2	0	
LC3	$1/8A_b$	
LC4	$1/4A_b$	Submerged
LC5	$1/2A_b$	
LC6	$5/8A_b$	

where k_i is the wave number derived from the dispersion equation. By solving the above equations, the phase ϕ_i can be derived.

The wave amplitude a_i is weighted according to the energy ratio, written as

$$a_i = A_{ab}\frac{S(f_i)}{\sum_{n=1}^{N} S(f_n)}, \tag{7}$$

where A_{ab} is the assumed focused amplitude, and $S(f)$ is the spectral density function using the advanced JONSWAP method.[37]

III. NUMERICAL SETUP

A. Numerical model

A two-dimensional numerical wave tank is established based on the CFD technique to simulate a floater under extreme wave conditions. The fluid domain is illustrated in Fig. 2, with a length of 18 m and a depth of 1 m. There are two 5-m-long wave-forcing zones set on the left and right sides, respectively. The left is to generate incident waves and the right is to absorb reflected waves. The prescribed focused waves are generated from the left side using the superposition VOF wave model.

The asymmetric floater with a triangular-baffle shaped bottom is selected as the research object, whose specific size can be referred to the partial view [Fig. 2(b)]. The front edge of the floater is placed at the actual focused position (x_b) in the horizontal direction and with various emerged/submerged depths related to the actual focused amplitude (A_b) listed in Table I. Case LC1 is taken for comparison, in which the floater is fixed with three degrees of freedom restricted when the

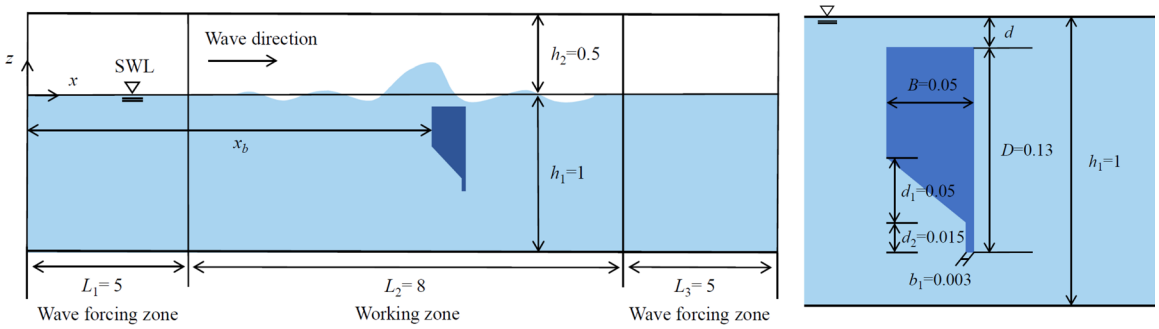

(a) the numerical tank (b) the partial view of the floater

FIG. 2. Schematic diagram of the numerical wave tank and the selected floater (unit: m).

TABLE II. Detailed mesh size for spatial convergence analysis.

Model	Time step	Mesh size of liquid level encryption zone	Mesh size of floating body encryption zone	Total number of meshes
Coarse	$\Delta t = T_p/1000$	$\Delta z = A_b/10$, $\Delta x = 4\Delta z$	$\Delta z = A_b/10$, $\Delta x = \Delta z$	87 239
Medium		$\Delta z = A_b/20$, $\Delta x = 4\Delta z$	$\Delta z = A_b/20$, $\Delta x = \Delta z$	325 733
Fine		$\Delta z = A_b/30$, $\Delta x = 4\Delta z$	$\Delta z = A_b/30$, $\Delta x = \Delta z$	708 715

extreme waves happen. In the table, d, defined as the distance between the top of the floater and the still water surface, is assumed to the positive when the floater is underwater, and otherwise is negative.

B. Convergence analysis

Convergence analysis of the established numerical model is to be conducted in this section. Three schemes listed in Table II with different mesh sizes in the vertical interval Δz are chosen to be compared, which is along with the mesh discretization in the x direction synchronized.

Focused waves with actual focused amplitude $A_b = 0.033$ m and peak frequency $f_p = 0.994$ Hz are used in the convergence test. The front edge of the floater is located 10.15 m away from the wavemaker, which is exactly the actual focused position, and the state of the floater emerges with $d = -A_b$. The comparisons of the water surface

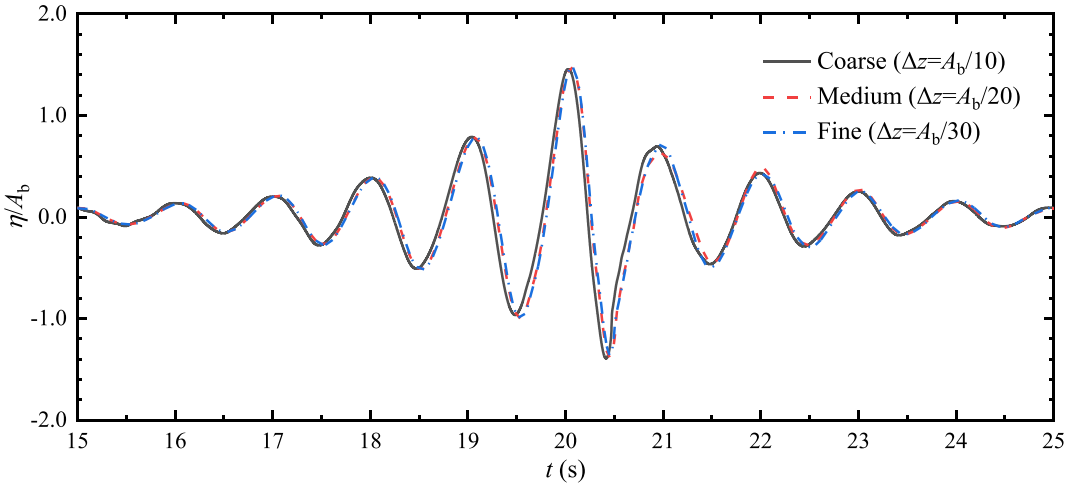

(a) Wave surface elevation at the position in front of the floater (x=10.1 m)

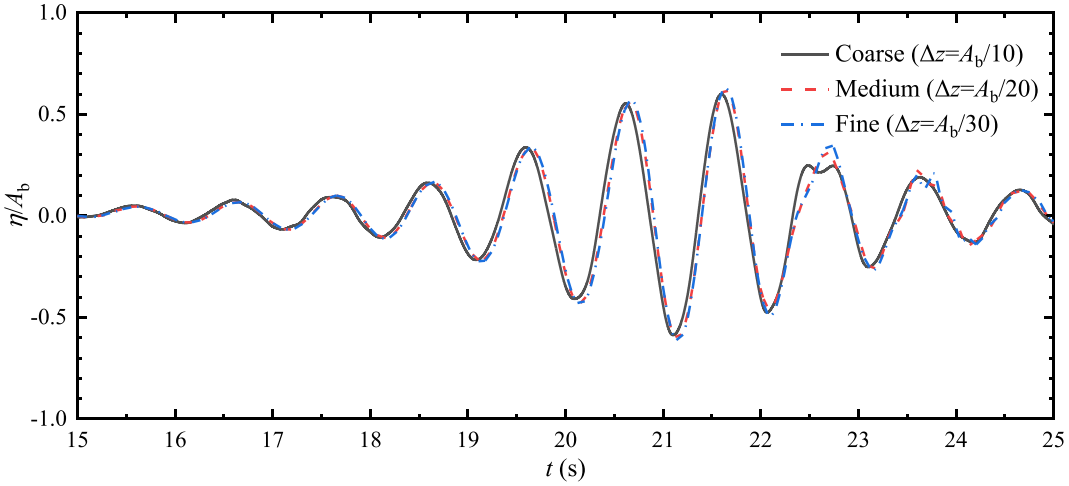

(b) Wave surface elevation at the position behind the floater (x=11 m)

FIG. 3. Comparison of the spatial convergence analysis.

elevation at the position in front of and behind the floater are given in Fig. 3. It can be found that the differences in the maximum in front of the floater between coarse ($\Delta z = A_b/10$) and medium ($\Delta z = A_b/20$), and medium ($\Delta z = A_b/20$) and fine ($\Delta z = A_b/20$) are 1.82% and 0.07%, and those behind the floater are 4.04% and 0.40%, respectively. Compared with the difference between the coarse and medium, that between medium and fine is small. Similarly, the convergence analysis in the time domain is given in Fig. 4. The intermediate time step $\Delta t = T_p/1000$ can satisfy the simulation accuracy. Hence, the steps in the spatial domain $\Delta z = A_b/20$ and in the time domain $\Delta t = T_p/1000$ are employed in this study.

C. Model validation

Using the discrete parameters obtained from the convergence analysis above, the focused waves are numerically simulated identical the same setup as the physical experiment conducted in the wave flume at the Ship and Ocean Engineering Laboratory, South China University of Technology, China. The comparison of the water surface elevation is given in Fig. 5. The difference around the focused time between the numerical results and experimental data is only 3.73%. The good agreement with the experimental data proves that the established numerical model can accurately reproduce extreme waves with strong nonlinearity.

For further verification, the physical experiment conducted by Rodríguez *et al.*[38] to investigate the wave loads on the fixed rectangular box caused by regular waves is used for comparison. Regular waves with wave steepness $kA = 0.1$ (k is the wave steepness and A is the wave amplitude of the regular wave) and a rectangular box with relative size $kb = 0.7$ (b is half of the length of the rectangular box). The comparison of total vertical forces between the numerical results and the experimental data is given in Fig. 6, where T is the period of regular waves and the vertical force is nondimensionalized by ρgAb. The calculation error relative to the experimental data (detailed in Ref. 39) is statistics as a value of 4.46%, which indicates that the numerical model

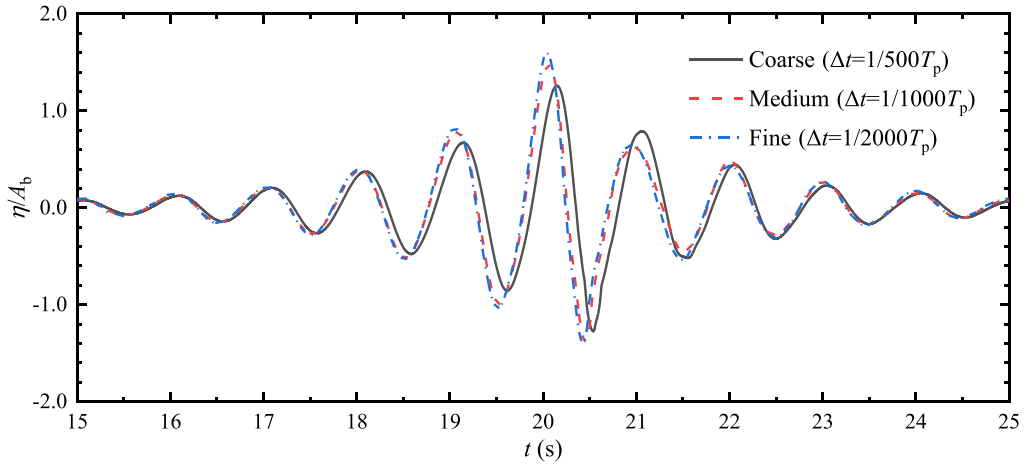

(a) Wave surface elevation at the position in front of the floater (x=10.1 m)

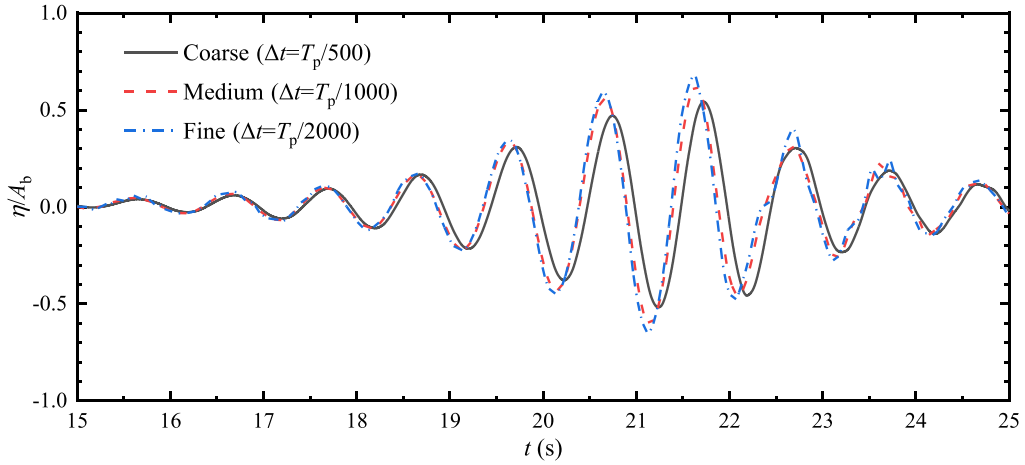

(b) Wave surface elevation at the position in front of the floater (x=11 m)

FIG. 4. Comparison of the convergence analysis in the time domain.

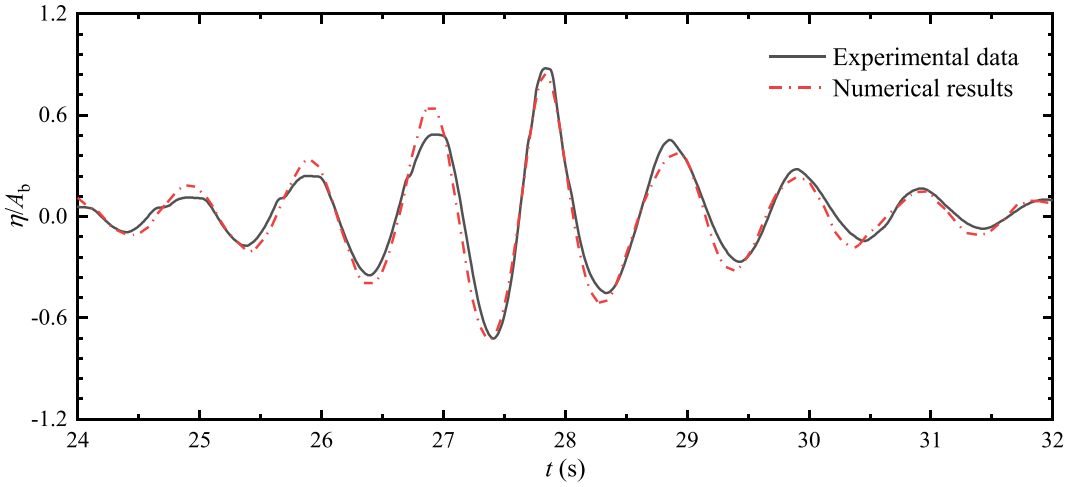

FIG. 5. Comparison of the wave surface elevation between numerical results and experimental data at the position $x = 9.9$ m ($A_{ab} = 0.04$ m, $f_p = 1.0$ Hz, $x_{ab} = 10$ m, $t_{ab} = 28$ s, $h = 1.0$ m).

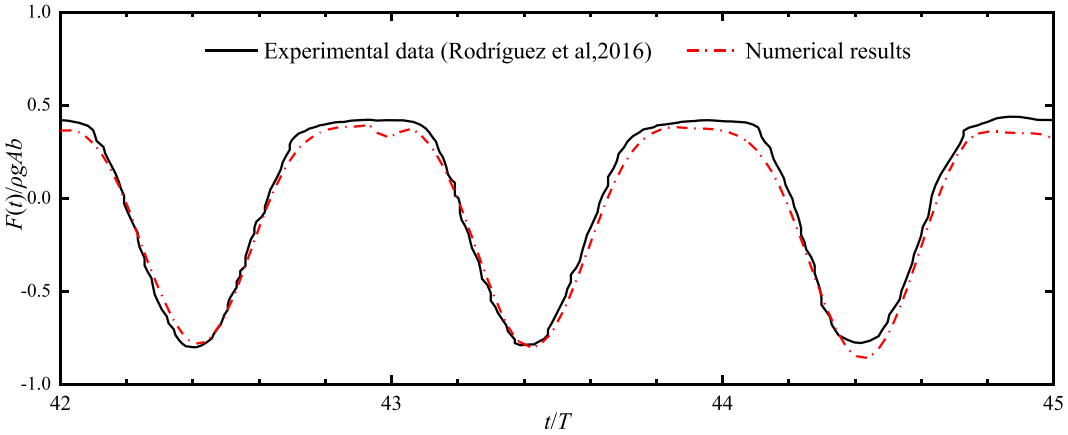

FIG. 6. Comparison of the total vertical force between numerical results and experimental data.

is capable of simulating the interaction between waves and floaters with sufficient accuracy.

D. Wave conditions

Five cases of wave configuration are chosen to study the impact of the wave parameters on the wave loads in the survival mode, as listed in Table III, in which the total wave components remain 81 unchanged. Waves in cases 1–3 with the same peak frequency but different focused amplitudes are used to investigate the effect of the focused amplitude, and cases 1, 4, and 5 with the same focused amplitude but the different peak frequencies to investigate the effect of the peak frequency.

TABLE III. Detailed parameters of various wave configurations.

Case	Actual focused amplitude, A_b (m)	Peak frequency, f_p (Hz)	Spectral range, Δf (Hz)	Actual wave steepness k_pA_b	Actual focused position, x_b (m)	Actual focused time, t_b (s)
1	0.038	0.994	0.6–1.8	0.15	10.20	20.07
2	0.043			0.17	10.25	20.10
3	0.058			0.23	10.40	20.14
4	0.038	0.894	0.5–1.7	0.12	10.25	20.11
5	0.038	1.120	0.7–1.9	0.19	10.25	20.08

IV. RESULTS AND ANALYSIS

The survivability of the wave energy converters depends on their load capacity under extreme sea conditions. Previous studies have suggested that placing the floater underwater can reduce the load force,[40] being an accepted positive strategy. To investigate the optimal submergence and the impact of the wave configuration on them, hereafter, total forces in the horizontal and vertical directions, as well as their component forces corresponding to each order at different submergences will be analyzed.

A. Analysis of wave load with different submergences

1. Total horizontal and vertical forces

Figure 7 compares variations of the time histories of total horizontal force F_x and total vertical force F_z influenced by submerged depths, in the wave state with actual focused amplitude $A_b = 0.038$ m and peak frequency $f_p = 0.994$ Hz (i.e., case 1). The horizontal force along the wave propagation is defined as positive and the vertical force upward is defined as positive; otherwise, it is negative. Note that the positive or the negative only represents the direction of the wave force, so the maximum magnitude of both positive and negative forces is essential to draw more attention. Therefore, their corresponding maximum magnitude of the positive and negative forces is collected in Fig. 8, where the subscripts p and t denote the peak and the trough.

Concerning the total horizontal force in Fig. 7(a), its time history tends similarly to that of the water surface elevation, manifested as the exhibition that the peak appears around the focused time along with asymmetry troughs on adjacent sides. Additionally, as the submerged depth becomes deeper, the magnitudes of the positive peaks as well as the negative trough become smaller. That also means that the magnitudes of the positive peaks in the submerged state (LC2–LC6) are decreased compared to that in the emerged state (LC1). It can be explained by the fact that when placing the floater underwater in extreme sea conditions at different water depths, the interaction surface between wave and structure remains unchanged, demonstrating that the horizontal forces on the floater depend on the wave pressure on the wavefront. As known, within a certain range of the water depth, the deeper the water depth, the smaller the horizontal velocity of water particles, and consequently, the smaller the wave pressure applied to the wavefront. The summary of the maximum magnitude of the horizontal forces (Fig. 8) also delivers this information on the attenuation

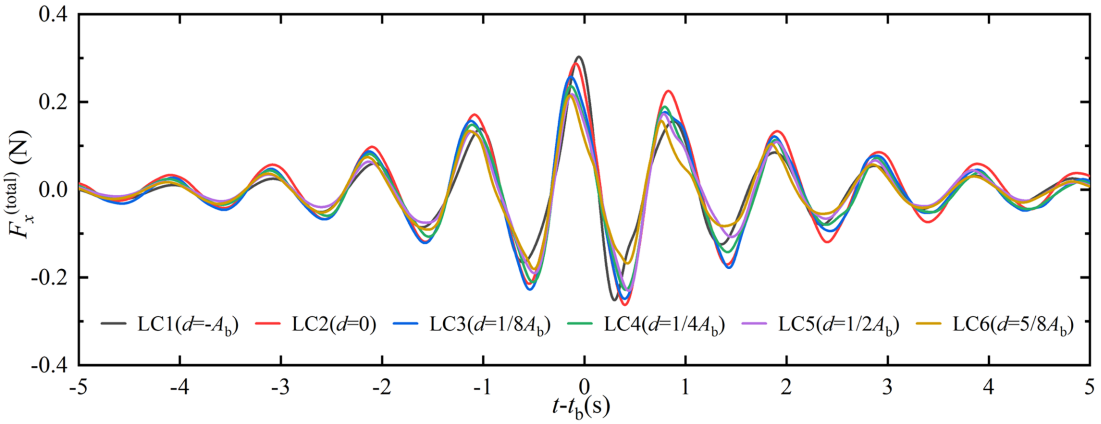

(a) Total horizontal forces

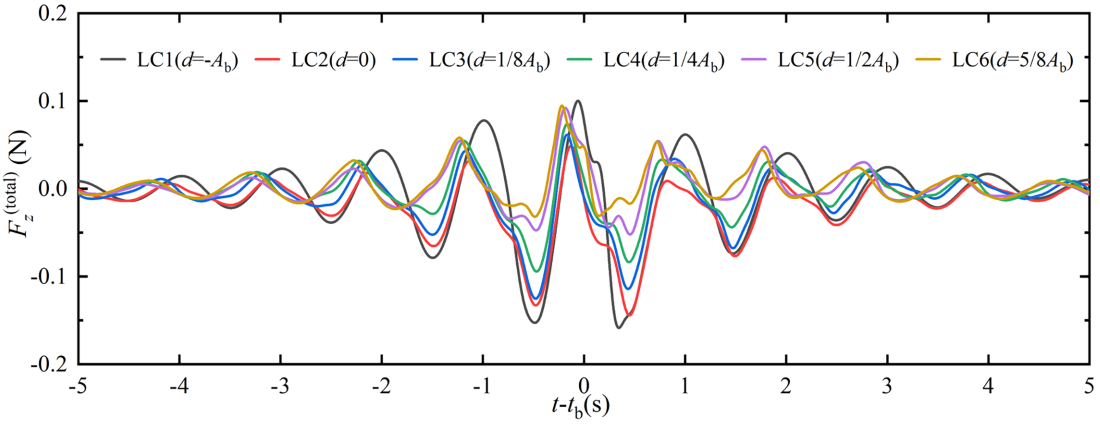

(b) Total vertical forces

FIG. 7. Influence of submerged depths on the time history of total wave forces in the wave state of case 1 ($A_b = 0.038$ m, $f_p = 0.994$ Hz).

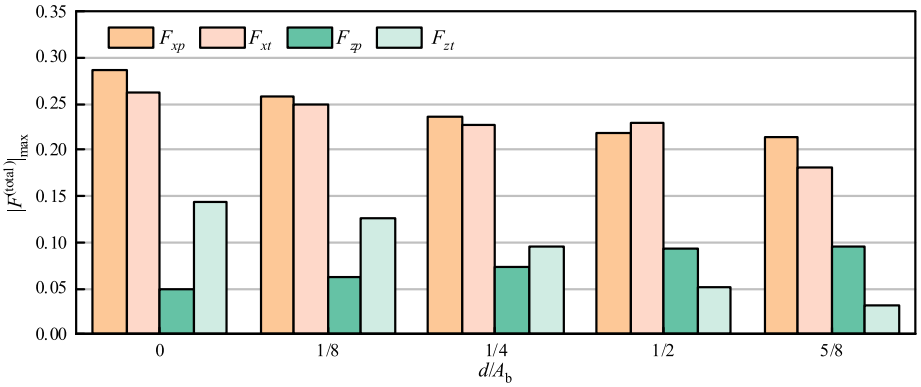

FIG. 8. Influence of submerged depths on the maximum magnitude of the peak (marked with the subscript *p*) and trough (marked with the subscript *t*) of total wave forces.

effect of deeper water depth on the horizontal forces containing the positive peak and the negative trough.

The variation of the total vertical force exhibits some differences [Fig. 7(b)]. In the state with the floater just submerged (LC2), the peak value of the total vertical forces rapidly decreases to the minimum of all. With the increase in the submergence, the peak value gradually increases again, and it is still below that in the emergent state when the submergence increases to the deepest (i.e., LC6: $5/8A_b$). For the trough, its magnitude decreases as the submergence keeps deepening. This monotonous variation of the vertical forces with the submerged depth can be considered as the combined action of hydrostatic pressure and hydrodynamic pressure. When the submerged floater interacts with the incident waves, the total vertical force comes from not only the hydrostatic pressure but also the hydrodynamic pressure. With the increase in the water depth, the hydrostatic pressure keeps increasing rapidly while the hydrodynamic pressure decreases slowly. This will lead to a minimum vertical total force occurring at some submerged depth.

From the above, placing the floater underwater in extreme sea conditions can indeed reduce the total horizontal force, and deepening the submergence can promote this effect within a certain range. Meanwhile, the decrease in total vertical force (including positive and negative values) will exhibit a midst mode, at which the magnitude can achieve its maximum within the given range of the submerged depth.

To quantitatively describe the effectiveness of the strategy of placing the floater underwater under extreme sea conditions, K_F, a parameter of the reduction ratio of wave force maximum magnitude, is defined hereafter in this study

$$K_F = \left(1 - \frac{|F^{(\text{total})}|_{\max}}{|F_e{}^{(\text{total})}|_{\max}}\right) \times 100\%, \tag{8}$$

where F_e represents the corresponding wave force in the emergent state (i.e., case 1, LC1).

Figure 9 summarizes the reduction ratio with different submergences. Although for total horizontal force, the reduction ratio can increase from 5.06% to 29.14% with the continued increase in the submerged depth, the reduction ratio in the total vertical force rapidly increases followed by slow decreases but remains above 40%. This phenomenon suggests that the strategy of placing the floater underwater can be quite beneficial in significantly reducing the total vertical forces. Moreover, the submergence state with the depth of $1/2A_b$ (i.e., LC5) having the advantage of reducing the total vertical force up to the maximum 41.89% and fine reduction capacity in total horizontal force can be supposed to be a more preferred candidate in promoting the survival performance.

2. Decomposed harmonic forces

When strong nonlinear extreme waves interact with a floater, the induced high-order wave loads (observed from the spectral analysis in Appendix A) cannot be ignored. In this study, based on the four-phase decomposition method (introduced in Appendix B), the total forces

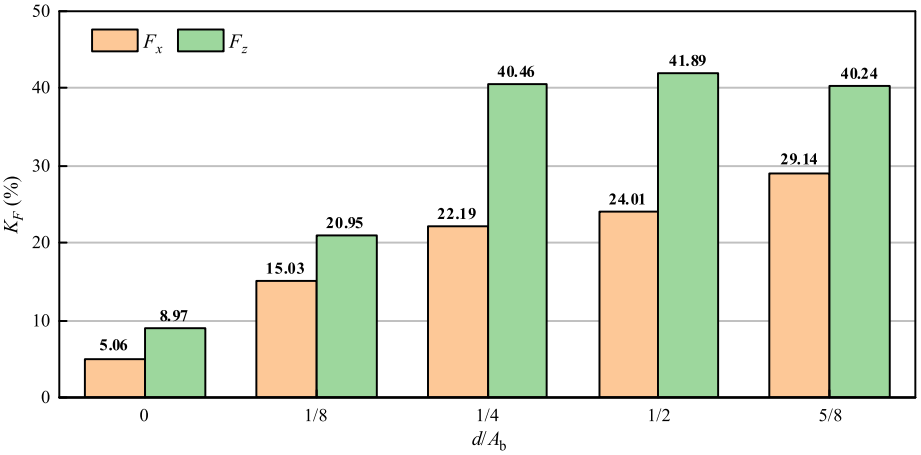

FIG. 9. Influence of submergences on the wave force magnitude reduction ratio.

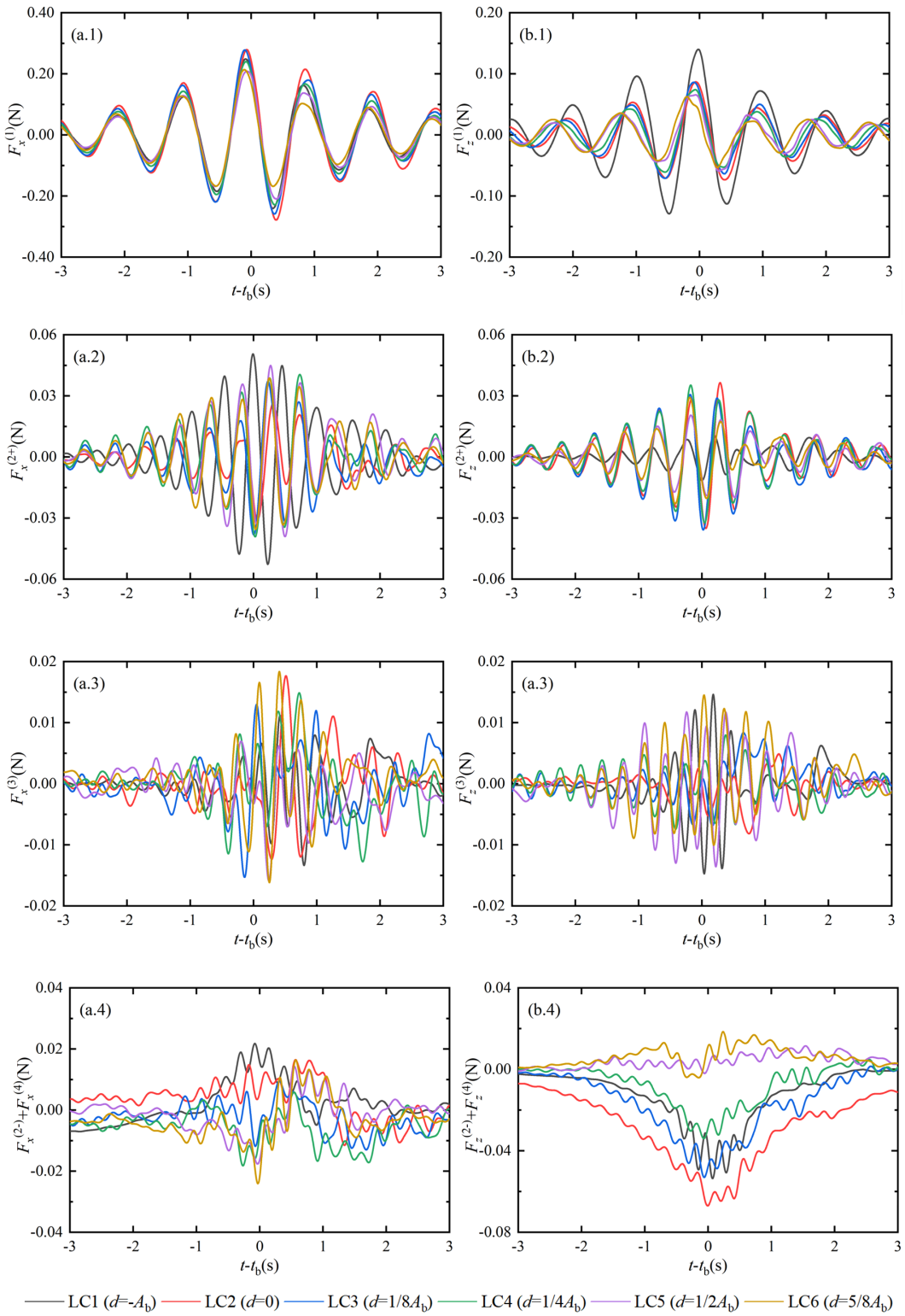

FIG. 10. Influence of submerged depths on the time history of each order harmonic wave force. Left (a) is the value of the horizontal wave force, and right (b) is the value of the vertical wave force. (1) The first-order term, (2) the second-order sum term, (3) the third-order term, and (4) the second-order difference and fourth-order term.

can be decomposed into the linear term $F^{(1)}$, the second-order sum term $F^{(2+)}$, the third-order term $F^{(3)}$, and the second-order difference and fourth-order term $F^{(2-)}+F^{(4)}$. The corresponding time histories with different submerged depths are compared in Fig. 10, in which the left represents the horizontal forces and the right represents the vertical forces.

Concerning the horizontal force illustrated in Fig. 10(a), the maximum magnitude of the linear force [Fig. 10(a.1)] near the focused time occurs when the floater is just submerged. With the increase in the submerged depth, the maximum value decreases and gradually becomes smaller than that in the emerged state when the submerged depth is larger than $1/4A_b$ (LC4). There is no significant change in the phase of the linear force between the submerged state and the emerged state, but it is different for the second-order sum force [Fig. 10(a.2)]. In the submerged state, there is a phase lag near π relative to that in the emerged state. That is, the maximum magnitude of the time history in the emerged state occurs at the peak, while it occurs at the trough in the submerged state, which dominates a decrease in the maximum of the total horizontal forces with the floater underwater. Meanwhile, the value of $F^{(2-)}+F^{(4)}$ at the focused time decreases and gradually turns from the positive into the negative with the increase in the submerged depth, also contributing to the reduction of the total force. In contrast, the third-order force has a negligible effect due to its smaller order of magnitude. Therefore, although the linear component increases when the floater is just submerged, the total horizontal force is smaller than that in the emerged state, reflecting that the influence of the submerged depth on the even order force [including $F^{(2+)}$ and $F^{(2-)}+F^{(4)}$] exceeds that on the linear force. As a result, different submerged depths have various effects on the total horizontal force.

For vertical forces that are more sensitive to the submerged depth [Fig. 10(b)], the peak as well as the trough of the linear forces are significantly reduced when the floater is placed underwater, and the reduction magnitude increases as the submerged depth increases. Similar to the horizontal force, the second-order sum force exhibits the trough at the focused time and their magnitudes occur in a decreasing trend with the increase in the submerged depth while remaining a much larger value than that in the emerged state. $F^{(2-)}+F^{(4)}$ behaviors monotonic variation with the change of the submerged depth. Once the floater is placed in a shallow water depth, the value of $F^{(2-)}+F^{(4)}$ is negative. The greater the submerged depth, the smaller the magnitude of $F^{(2-)}+F^{(4)}$, until the relative submerged depth is greater than 0.25 at which point the magnitude is smaller than that in the emerged state. While placed in deep water (i.e., d/A_b is greater than 0.5), the value of $F^{(2-)}+F^{(4)}$ covers a smaller positive. The above phenomenon illustrated that the trends of the linear force and the second-order force vary monotonically with the change of the submerged depth, which does not agree with that of the total vertical force. Hence, it can be known that the effect of $F^{(2-)}+F^{(4)}$ cannot be ignored, which further indicates that the linear theory cannot lead to reliable results to predict the force loads of the floater under extreme circumstances.

B. Analysis of wave loads with different focused amplitudes

Based on the above analysis, placing the floater underwater with a depth of 0.5 times the actual wave amplitude in the given sea state achieves better wave force reduction. To investigate the universality of this so-called optimal submerged depth, three case wave configurations (i.e., cases 1–3 listed in Table III) with the same peak frequency but different incident amplitudes are selected to study.

Figure 11 compares the reduction ratio of the wave force magnitude with various wave amplitudes. As the actual wave amplitude increases from 0.038 to 0.058 m, the decrease in the reduction ratio of the total vertical force is 12.51%, greater than the decrease with a value of 2.75% concerning the total horizontal force. However, for larger waves, the effectiveness of this strategy of placing the floater underwater half the actual wave amplitude to reduce the wave loads will be weakened a bit. For the case with the largest wave amplitude, whose actual wave steepness has reached up to 0.23, the reduction of the wave force is not as good as the case with a smaller wave amplitude, but also remarkable with a reduction near 30% of the total vertical force and 22% of the total horizontal force.

From the view of the finite amplitude theory, the increase in the incident wave amplitude with fixed peak frequency means the increase in the wave steepness, consequently causing a larger horizontal velocity and pressure of water particles. However, the submerged state holds a larger wave-facing surface and smaller horizontal pressure compared to the emerged state. This leads to a reduction ratio of the wave force magnitude decreased for larger wave amplitude despite the increased total horizontal force. For vertical direction, the larger the incident

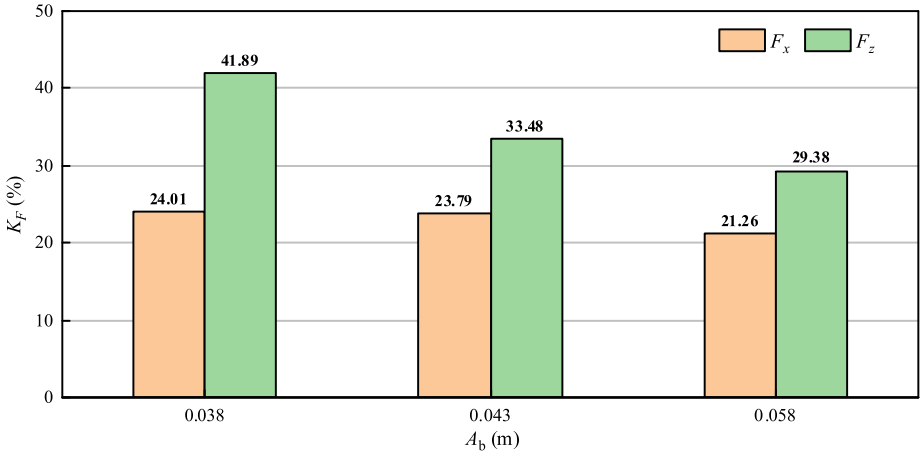

FIG. 11. Influence of different focused amplitudes on the wave force magnitude reduction ratio.

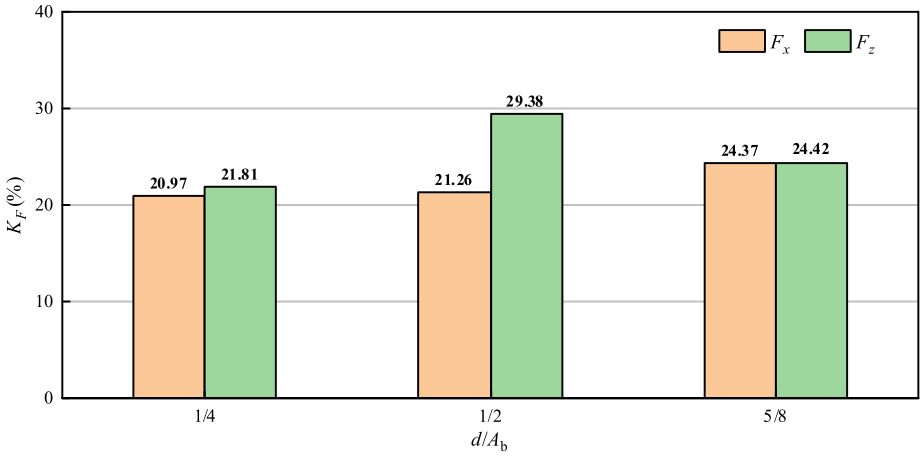

FIG. 12. Influence of submerged depth on the wave force magnitude reduction ratio in more extreme wave conditions ($A_b = 0.058$ m).

wave amplitude, the greater the vertical hydrodynamic pressure. When a floater placed underwater at the same submerged depth is subjected to various waves with different incident wave amplitudes, the total vertical force of the configuration with higher hydrodynamic pressure is naturally higher for their hydrostatic pressure remains the same. The rapid increase in total vertical force leads to a significant decrease in the reduction ratio. The above phenomenon reflects the variation in the reduction ratio of the wave force magnitude with the incident wave amplitude is not linear. When considering extreme waves characterized by strong nonlinearity, higher-order wave loads may be induced, which cannot be ignored in practical engineering applications.

Considering that case 3 is more representative of extreme sea conditions for larger actual wave steepness and its wave force reduction is much worse, the influence of the submerged depth is worth further testing. From the comparison shown in Fig. 12, it can be observed that the reduction ratio of the vertical wave force magnitude at the submerged depth of $1/2A_b$ is larger than that at the depth of $1/4A_b$ as well as $5/8A_b$, although the reduction ratio of the horizontal wave force is increasing with the increase in the submerged depth. This variation is similar to that in the wave configuration with a smaller incident wave amplitude (shown in Fig. 9). Hence, for priority to the vertical wave force, the optimal strategy in this wave condition is still preferred to placing the floater underwater at the submerged depth of $1/2A_b$. From this point of view, it can be pointed out that changes in the focused amplitude within a certain range hardly influence the optimal submerged depth despite the decrease in the magnitude reduction ratio (associated with the enhancement of the wave nonlinearity).

C. Analysis of wave loads with different peak frequencies

The influence of peak frequencies is to be illustrated in Fig. 13, based on three cases of wave configurations (i.e., cases 1, 4, and 5 listed in Table III) with the same focused amplitude but different peak frequencies. The larger the peak frequency (the shorter the wavelength), the larger the reduction ratio of horizontal force magnitude and the smaller the reduction ratio of vertical force magnitude. This means that placing the floater underwater at a certain depth is beneficial to decrease the vertical loads with a ratio value above 40%, especially in longer wave conditions, and the reduction ratio of horizontal force is increased in shorter wave conditions. Under the assumption that the front of the floater is exactly arranged at the position with wave focused, the phase at this position remains consistent under different

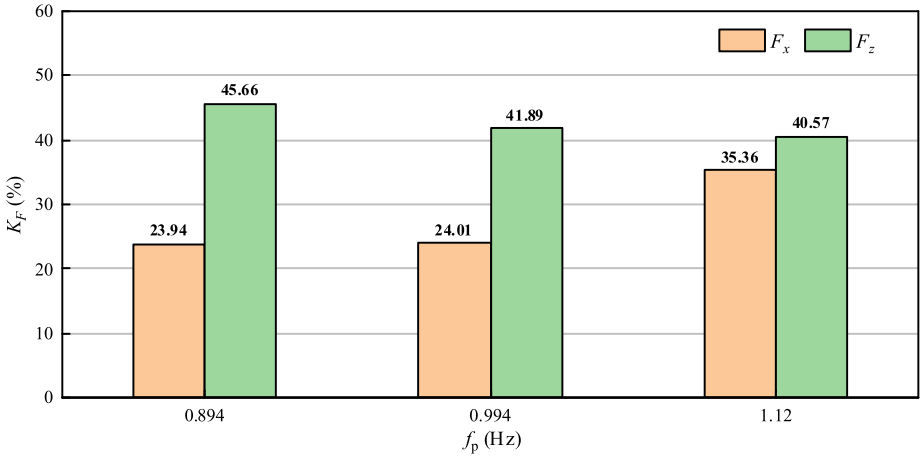

FIG. 13. Influence of different peak frequencies on the wave force magnitude reduction ratio.

wave conditions so that the horizontal velocity of the wave particles is proportional to the peak frequency. That is, the higher the peak frequency, the greater the horizontal velocity of the wave particles. It demonstrates that the horizontal force under shorter wave conditions should be greater when the floater is placed underwater at the same submerged depth, while here the reduction ratio is larger. It may be related to the increase in the horizontal force in the emerged state. Concerning the vertical force, the larger the peak frequency (i.e., shorter wavelength), the larger the wave steepness, while the smaller the reduction ratio. Although the range difference in actual wave steepness caused by the variation in peak frequency (i.e., cases 1, 4, and 5, from 0.12 to 0.19) and that in the focused wave amplitude (i.e., cases 1–3, from 0.15 to 0.23) is little, the corresponding variation in the reduction ratio of horizontal and vertical wave force magnitude is quite different. That is, the corresponding decrease in the reduction ratio of horizontal and vertical wave force magnitude are −11.42% and 5.09% with the increase in the peak frequency and compared to those values 2.75% and 12.51% with the increase in the focused amplitude. This suggests that the wave conditions with larger focused amplitude should be paid more attention to for the variation of wave force reduction is more sensitive to changes in focused amplitude in such a given configuration.

V. CONCLUSIONS

This paper numerically investigates the wave forces on a floater (including both total forces and various harmonic forces) at different submerged depths to identify an optimal survival strategy in response to extreme wave conditions. The main findings are summarized as follows:

(1) The patterns of variation for horizontal and total vertical forces as influenced by submerged depth differ in the specified sea state. The peaks and troughs of the total horizontal force diminish as submerged depth increases, whereas for the total vertical force, deeper submergence results in higher peaks and lower troughs.
(2) Placing the floater underwater at the depth of $1/2A_b$ (where A_b represents the actual focused amplitude of the incident waves) is confirmed as the optimal strategy for maximizing wave force reduction in the given sea state. As submerged depth increases, the magnitude of the total horizontal force lessens, and the total vertical force initially rises then falls, indicating that a depth of $1/2A_b$ offers the most effective wave force reduction vertically and excellent performance horizontally.
(3) While even order forces [including $F^{(2+)}$ and $F^{(2-)}+F^{(4)}$] predominantly influence the total horizontal force, the second-order difference and the forth-order forces [$F^{(2-)}+F^{(4)}$] play a significant role in the variation of total vertical forces. Relying solely on linear terms for the total horizontal force or on linear and second-order sum terms for the total vertical force does not accurately capture the variations, suggesting that linear theory is insufficient for predicting wave loads.
(4) The optimal performance in wave force reduction under more extreme conditions, with an actual wave steepness of k_pA_b at 0.23, remains at a submerged depth of $1/2A_b$, showing reductions of 21.26% and 29.38% in the horizontal and vertical directions, respectively. Wave conditions with larger focused amplitudes warrant closer attention, as the variation in wave force reduction is more sensitive to changes in focused amplitude than to shifts in peak frequencies for this particular configuration.

These insights delineate the optimal submerged depth for responding to extreme wave conditions and the influence of wave conditions on this response, which is advantageous for the survival mode planning of marine devices. This guidance is instrumental in designing devices with enhanced reliability. In the future, the device considering the effect of the mooring and even the hybrid system combining the floater with floating breakwaters or platforms will be noticed. The research on their survival strategy in more complex extreme waves is going to be pushed ahead. This will better guide practical engineering.

ACKNOWLEDGMENTS

This work is supported by the National Key R&D Program of China (No. 2023YFB4204101), the National Natural Science Foundation of China (Nos. 52301319 and 52071096), the National Natural Science Foundation of China National Outstanding Youth Science Fund Project (No. 52222109), Guangdong Basic and Applied Basic Research Foundation (No. 2022B1515020036), Guangzhou Basic and Applied Basic Research Foundation (No. 2023A04J1596), Project of State Key Laboratory of Subtropical Building and Urban Science (No. 2023ZB14), and the Open Research Fund of Guangdong Provincial Key Laboratory of Marine Disaster Prediction and Prevention (No. GPKLMD2023006).

AUTHOR DECLARATIONS

Conflict of Interest

The authors have no conflicts to disclose.

Author Contributions

Binzhen Zhou: Funding acquisition (equal); Project administration (equal); Supervision (lead); Writing – review & editing (equal). **Yi Xiao:** Conceptualization (equal); Data curation (lead); Investigation (lead); Methodology (equal); Visualization (equal); Writing – original draft (lead). **Kanglixi Ding:** Formal analysis (equal); Investigation (equal); Writing – review & editing (equal). **Lei Wang:** Conceptualization (equal); Formal analysis (equal); Funding acquisition (equal); Methodology (equal); Writing – review & editing (lead). **Yifeng Yang:** Investigation (equal); Writing – review & editing (equal). **Peng Jin:** Conceptualization (equal); Writing – review & editing (equal).

DATA AVAILABILITY

The data that support the findings of this study are available from the corresponding author upon reasonable request.

APPENDIX A: FORCE ENERGY SPECTRUM

Fast Fourier transform (FFT) is an important tool for reflecting energy distribution in the frequency domain. Figure 14 compares the spectral characteristics of the total forces in different submerged depths, in which the vertical value is normalized by the corresponding total force maximum ($[S_e(f)]_{max}$) in the emerged state. Concerning the

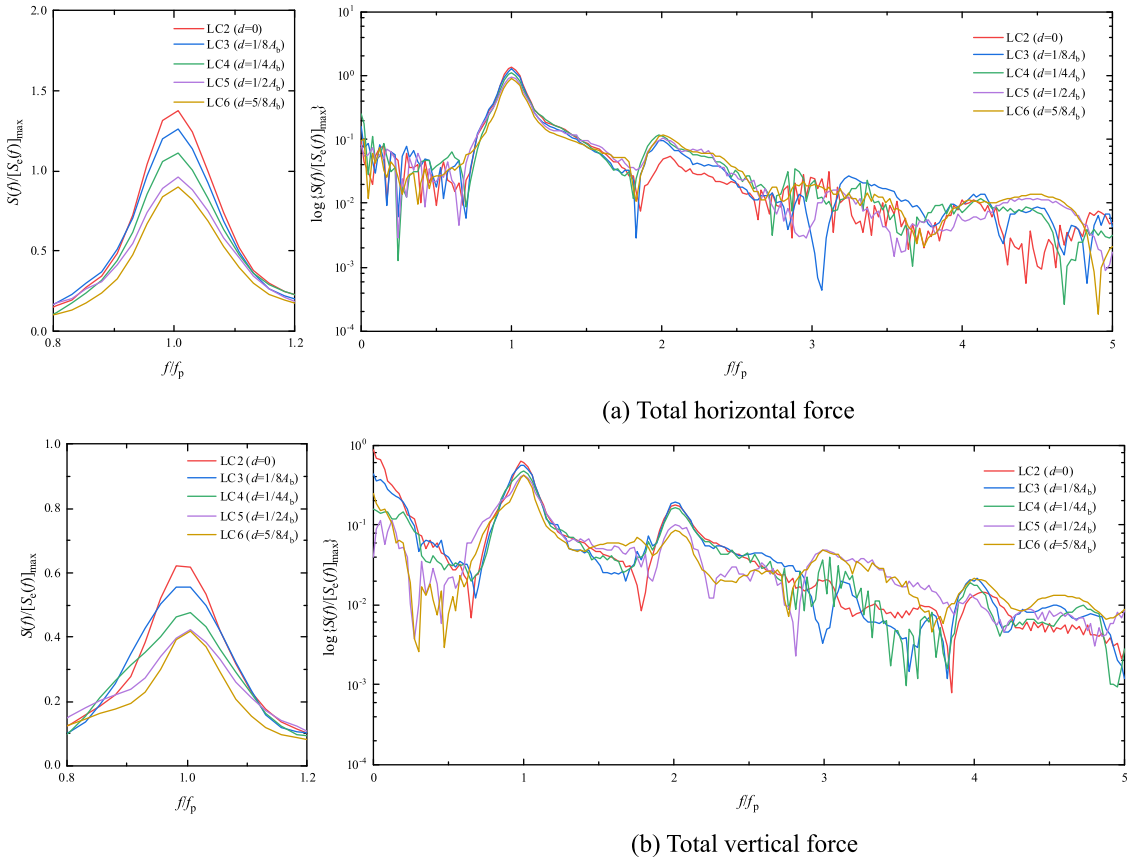

FIG. 14. Influence of different submerged depths on the force energy spectrum (case 1).

horizontal force [Fig. 14(a)], the peak in the fundamental frequency range achieves a maximum in the just submerged state (i.e., LC2), and then decreases gradually with the increase in the submergence depth. When the relative submerged depth is greater than 1/2, the peak value begins to be less than that in the emerged state. The high-order components hardly change with the variation of the submerged depth. For the vertical force [Fig. 14(b)], the peak in the fundamental frequency range achieves a maximum also in the just submerged state (i.e., LC2), and then decreases gradually with the increase in the submergence depth. Differently, the peak values in the submerged state are much smaller than that in the emerged state. When the submerged depth is greater than 1/2, the peak value tends to be stable. Additionally, there are also some differences in the second-order difference components and high-order harmonics, which should not be ignored in the analysis.

APPENDIX B: FOUR-PHASE DECOMPOSITION METHOD

According to Stokes wave theory, the water surface elevation can be expanded into several high-order components[30,41]

$$\eta = A\eta_{11}\cos(\theta) + A^2(\eta_{20} + \eta_{22}\cos(2\theta)) + A^3(\eta_{31}\cos(\theta) + \eta_{33}\cos(3\theta)) + A^4(\eta_{40} + \eta_{42}\cos(2\theta) + \eta_{44}\cos(4\theta)) + O(A^5), \tag{B1}$$

where A denotes the wave amplitude, θ denotes the wave phase, and η_{ij} denotes the jth term of the ith order component. Similarly, when the waves interact with the marine structure, the high-order wave loads can be written as[32]

$$F = AF_{11}\cos(\theta) + A^2(F_{20} + F_{22}\cos(2\theta)) + A^3(F_{31}\cos(\theta) + F_{33}\cos(3\theta)) + A^4(F_{40} + F_{42}\cos(2\theta) + F_{44}\cos(4\theta)) + O(A^5). \tag{B2}$$

According to the four-phase decomposition method applied to the wave surface elevation,[42] when the phase is assigned the value of 0, $\pi/2$, π, and $3\pi/2$, the expression of F_0, F_{90}, F_{180}, and F_{270} can be consequently obtained. Then, the linear and nonlinear harmonics can be obtained based on the following:

$$\begin{aligned} F^{(1)} &= \frac{F_0 + iF_{90} - F_{180} - iF_{270}}{4}, \\ F^{(2)} &= \frac{F_0 - F_{90} + F_{180} - F_{270}}{4}, \\ F^{(3)} &= \frac{F_0 - iF_{90} - F_{180} + iF_{270}}{4}, \\ F^{(2-)} + F^{(4)} &= \frac{F_0 + F_{90} + F_{180} + F_{270}}{4}, \end{aligned} \tag{B3}$$

where $F^{(1)}$, $F^{(2)}$, $F^{(3)}$, and $F^{(2-)}+F^{(4)}$ represent the linear force, the second-order sum force, the third-order force, and the second-order difference and fourth-order force, respectively.

REFERENCES

[1]J. Falnes, "A review of wave-energy extraction," Mar. Struct. **20**(4), 185–201 (2007).
[2]R. Alamian, R. Shafaghat, M. Shadloo *et al.*, "An empirical evaluation of the sea depth effects for various wave characteristics on the performance of a point absorber wave energy converter," Ocean Eng. **137**, 13–21 (2017).
[3]P. Sun, S. Hu, H. He *et al.*, "Structural optimization on the oscillating-array-buoys for energy-capturing enhancement of a novel floating wave energy converter system," Energy Convers. Manage. **228**, 113693 (2021).
[4]R. Ji, Q. Sheng, S. Wang *et al.*, "Array characteristics of oscillating-buoy two-floating-body wave-energy converter," J. Mar. Sci. Appl. **18**, 325–333 (2019).
[5]T. Heath, "A review of oscillating water columns," Philos. Trans. R. Soc. A **370**(1959), 235–245 (2012).
[6]A. Falcão and J. Henriques, "Oscillating-water-column wave energy converters and air turbines: A review," Renewable Energy **85**, 1391–1424 (2016).
[7]K. Monk, Q. Zou, and D. Conley, "An approximate solution for the wave energy shadow in the lee of an array of overtopping type wave energy converters," Coastal Eng. **73**, 115–132 (2013).
[8]L. Margheritini, D. Vicinanza, and P. Frigaard, "SSG wave energy converter: Design, reliability and hydraulic performance of an innovative overtopping device," Renewable Energy **34**(5), 1371–1380 (2009).
[9]C. Kharif and E. Pelinovsky, "Physical mechanisms of the rogue wave phenomenon," Eur. J. Mech. B **22**(6), 603–634 (2003).
[10]L. Wang, K. Ding, B. Zhou *et al.*, "Quantitative prediction of the freak wave occurrence probability in co-propagating mixed waves," Ocean Eng. **271**, 113810 (2023).
[11]B. Zhou, J. Hu, K. Sun *et al.*, "Motion response and energy conversion performance of a heaving point absorber wave energy converter," Front. Energy Res. **8**, 553295 (2020).
[12]B. Zhou, J. Hu, Q. Zhang *et al.*, "Optimal design and performance analysis of a hybrid system combining a semi-submersible wind platform and point absorbers," J. Mar. Sci. Eng. **11**(6), 1190 (2023).
[13]I. López, J. Andreu, S. Ceballos *et al.*, "Review of wave energy technologies and the necessary power-equipment," Renewable Sustainable Energy Rev. **27**, 413–434 (2013).
[14]M. Mustapa, O. Yaakob, Y. Ahmed *et al.*, "Wave energy device and breakwater integration: A review," Renewable Sustainable Energy Rev. **77**, 43–58 (2017).
[15]B. Zhou, Q. Zhang, P. Jin *et al.*, "Geometric asymmetry in the energy conversion and wave attenuation of a power-take-off-integrated floating breakwater," Ocean Eng. **246**, 110576 (2022).
[16]D. Ning, X. Zhao, M. Göteman *et al.*, "Hydrodynamic performance of a pile-restrained WEC-type floating breakwater: An experimental study," Renewable Energy **95**, 531–541 (2016).
[17]X. Zhao, D. Ning, C. Zhang *et al.*, "Hydrodynamic investigation of an oscillating buoy wave energy converter integrated into a pile-restrained floating breakwater," Energies **10**(5), 712 (2017).
[18]F. Madhi, M. Sinclair, and R. Yeung, "The "Berkeley Wedge": an asymmetrical energy-capturing floating breakwater of high performance," Mar. Syst. Ocean Technol. **9**, 5–16 (2014).
[19]H. Zhang, B. Zhou, C. Vogel *et al.*, "Hydrodynamic performance of a floating breakwater as an oscillating-buoy type wave energy converter," Appl. Energy **257**, 113996 (2020).
[20]Y. Wei, S. Yu, X. Li *et al.*, "Hydrodynamic analysis of a heave-hinge wave energy converter combined with a floating breakwater," Ocean Eng. **293**, 116618 (2024).
[21]Y. Cheng, C. Xi, S. Dai *et al.*, "Wave energy extraction and hydroelastic response reduction of modular floating breakwaters as array wave energy converters integrated into a very large floating structure," Appl. Energy **306**, 117953 (2022).
[22]S. Weller, T. Stallard, and P. Stansby, "Experimental measurements of the complex motion of a suspended axisymmetric floating body in regular and near-focused waves," Appl. Ocean Res. **39**, 137–145 (2013).
[23]S. A. Sirigu, M. Bonfanti, E. Begovic *et al.*, "Experimental investigation of the mooring system of a wave energy converter in operating and extreme wave conditions," J. Mar. Sci. Eng. **8**(3), 180 (2020).
[24]Z. Shahroozi, M. Göteman, and J. Engström, "Experimental investigation of a point-absorber wave energy converter response in different wave-type representations of extreme sea states," Ocean Eng. **248**, 110693 (2022).
[25]P. Ropero-Giralda, A. Crespo, B. Tagliafierro *et al.*, "Efficiency and survivability analysis of a point-absorber wave energy converter using DualSPHysics," Renewable Energy **162**, 1763–1776 (2020).
[26]F. Madhi and R. Yeung, "On survivability of asymmetric wave-energy converters in extreme waves," Renewable Energy **119**, 891–909 (2018).
[27]A. Borthwick, A. Hunt, T. Feng *et al.*, "Flow kinematics of focused wave groups on a plane beach in the UK Coastal Research Facility," Coastal Eng. **53**(12), 1033–1044 (2006).
[28]D. Ning, J. Zang, S. Liu *et al.*, "Free-surface evolution and wave kinematics for nonlinear uni-directional focused wave groups," Ocean Eng. **36**(15–16), 1226–1243 (2009).
[29]J. Zang, P. Taylor, G. Morgan *et al.*, "Experimental study of non-linear wave impact on offshore wind turbine flundations," in Coastlab10—3rd International Conference on the Application of Physical Modelling to Port and Coastal Protection (2010).
[30]L. Chen, J. Zang, P. Taylor *et al.*, "An experimental decomposition of nonlinear forces on a surface-piercing column: Stokes-type expansions of the force harmonics," J. Fluid Mech. **848**, 42–77 (2018).
[31]C. Fitzgerald, P. Taylor, R. Taylor *et al.*, "Phase manipulation and the harmonic components of ringing forces on a surface-piercing column," Proc. R. Soc. A **470**(2168), 20130847 (2014).
[32]X. Feng, P. Taylor, S. Dai *et al.*, "Experimental investigation of higher harmonic wave loads and moments on a vertical cylinder by a phase-manipulation method," Coastal Eng. **160**, 103747 (2020).
[33]Siemens, *Simcenter STAR-CCM+ User Guide, Version 18.02.008-R8* (Siemens, 2023).
[34]R. Bilandi, S. Jamei, F. Roshan *et al.*, "Numerical simulation of vertical water impact of asymmetric wedges by using a finite volume method combined with a volume-of-fluid technique," Ocean Eng. **160**, 119–131 (2018).
[35]J. Kim, J. O'Sullivan, and A. Read, "Ringing analysis of a vertical cylinder by Euler overlay method," in *International Conference on Offshore Mechanics and Arctic Engineering* (American Society of Mechanical Engineers, 2012), pp. 855–866.
[36]M. Longuet-Higgins, "On the statistical distributions of sea waves," J. Mar. Res. **11**(3), 245–265 (1952).
[37]Y. Goda, "A comparative review on the functional forms of directional wave spectrum," Coastal Eng. J. **41**(1), 1–20 (1999).
[38]M. Rodríguez and J. Spinneken, "A laboratory study on the loading and motion of a heaving box," J. Fluids Struct. **64**, 107–126 (2016).
[39]G. Ducrozet, F. Bonnefoy, D. Le Touzé *et al.*, "A modified high-order spectral method for wavemaker modeling in a numerical wave tank," Eur. J. Mech. B **34**, 19–34 (2012).
[40]P. Brevig, M. Greenhow, and T. Vinje, "Extreme wave forces on submerged wave energy devices," Appl. Ocean Res. **4**(4), 219–225 (1982).
[41]W. Shi, X. Zeng, X. Feng *et al.*, "Numerical study of higher-harmonic wave loads and runup on monopiles with and without ice-breaking cones based on a phase-inversion method," Ocean Eng. **267**, 113221 (2023).
[42]D. Stagonas and P. Higuera, "Simulating breaking focused waves in CFD: Methodology for controlled generation of first and second order," J. Waterway Port Coastal Ocean Eng. **144**(2), 06017005 (2018).